Journal of Medicinal Chemistry

Article

Exploring the Natural Piericidins as Anti-Renal Cell Carcinoma Agents Targeting Peroxiredoxin 1

Xuefeng Zhou, Zhi Liang, Kunlong Li, Wei Fang, Yuanxin Tian, Xiaowei Luo, Yulian Chen, Zhikun Zhan, Tao Zhang, Shengrong Liao, Shuwen Liu, Yonghong Liu, William Fenical, and Lan Tang

J. Med. Chem., **Just Accepted Manuscript** • DOI: 10.1021/acs.jmedchem.9b00598 • Publication Date (Web): 12 Jul 2019

Just Accepted

is published by the American Chemical Society. 1155 Sixteenth Street N.W., Washington, DC 20036

Exploring the Natural Piericidins as Anti-Renal Cell Carcinoma Agents Targeting Peroxiredoxin 1

Xuefeng Zhou,*[,†,#] Zhi Liang,[‡,#] Kunlong Li,[†] Wei Fang,[§] Yuanxin Tian[‡], Xiaowei Luo,[†] Yulian Chen,[‡] Zhikun Zhan,[‡] Tao Zhang,[‡] Shengrong Liao,[†] Shuwen Liu,[‡,⊥] Yonghong Liu,[†] William Fenical,[∥] and Lan Tang*[,‡,⊥]

[†]CAS Key Laboratory of Tropical Marine Bio-resources and Ecology, Guangdong Key Laboratory of Marine Materia Medica, South China Sea Institute of Oceanology, Chinese Academy of Sciences, Guangzhou 510301, China

[‡]Biopharmaceutics, Guangdong Provincial Key Laboratory of New Drug Screening, School of Pharmaceutical Sciences, Southern Medical University, Guangzhou 510515, China

[§]Hubei Biopesticide Engineering Research Center, Hubei Academy of Agricultural Science, Wuhan 430064, China

[⊥]State Key Laboratory of Organ Failure Research, Southern Medical University, Guangzhou 510515, China

[∥]Center for Marine Biotechnology and Biomedicine, Scripps Institution of Oceanography, University of California at San Diego, La Jolla, CA 92093, USA

KEYWORDS: Piericidins; renal cell carcinoma; ACHN; peroxiredoxin 1

ABSTRACT

Anti-renal cell carcinoma (RCC) agents with new mechanisms of action are urgently needed. Twenty seven natural products of the piericidin class, including seventeen new ones, are obtained from a marine-derived *Streptomyces* strain, and several of them show strong inhibitory activities against ACHN renal carcinoma cells. By exploring the mechanisms of two representative natural piericidin compounds, piericidin A (PA) and glucopiericidin A (GPA), peroxiredoxin 1 (PRDX1) is detected as a potential target by transcriptome data of PA treated ACHN cells, as well as the paired RCC tumor *vs* adjacent non-tumor tissues. PA and GPA induce cell apoptosis through reducing ROS level caused by up-regulated PRDX1 mRNA and protein level subsequently, and exhibit potent anti-tumor efficacy in nude mice bearing ACHN xenografts, with increasing PRDX1 expression in tumor. The interaction between PA/GPA and PRDX1 was supported by the docking analysis and SPR. Moreover, the translocation of PRDX1 into the nucleus forced by PA/GPA is proposed to be a key factor for the anti-RCC procedure. Piericidins provide a novel scaffold for further development of potent anti-RCC agents, and the new action mechanism of these agents targeting PRDX1, may improve upon the limitations of existing targeted drugs for the treatment of renal cancer.

1. Introduction

Renal cell carcinoma (RCC) is the most common form of renal cancer, whose incidence rates have been gradually increasing by 2–4% every year over the past few decades.[1] Chemotherapy and radiotherapy are not as successful in the case of RCC, although significant advances have been derived from several target drugs approved by the FDA, such as sorafenib, sunitinib, and pazopanib as tyrosine kinase inhibitors.[2] In order to curb drug resistance, unwanted side effects, and further improve efficacy, the discovery of more effective anti-RCC agents, especially those with novel mechanisms of action, is warranted.[3] The revolutionary technology employed in medicine to interrogate human cancer is next-generation sequencing, which enabled a hitherto unknown insight into the molecular and cellular machineries in RCC.[4] Further studies to dissect out the role of the mutated genes or key biomarkers in RCC tumorigenesis revealed by different genomic platforms will hopefully provide the foundation for the development of effective forms of therapy for this disease.[5]

Microorganisms remain unrivalled in their potential to produce highly potent natural products for drug development, and the actinomycetes are well-known as an inexhaustible source for new chemical structures. The piericidin class metabolites, that feature a 4-pyridinol core linked with a variable polyene side chain, are commonly produced by actinomycetes isolated from soil, insects and marine samples.[6] To date, there are about 40 natural piericidin derivatives reported, including 11 piericidin glycosides.[6-8] Piericidin A (PA) is known as a potent inhibitor of NADH−ubiquinone oxidoreductase (complex I). In addition to broad antimicrobial and insecticidal activities, some piericidins are reported to have potential as antitumour agents.[6] The chemical diversity of the natural piericidins has not been reached, thus the pharmaceutical

significance of this class will require further refinement and examination, especially regarding their anticancer mechanisms of action.

Described herein is the isolation and structure determination of 27 natural piericidins from a *Streptomyces* strain, with inhibitory activities against RCC ACHN cells. Driven by transcriptomic analysis, a new action mechanism for the piericidins, targeting the anti-oxidative protein peroxiredoxin 1 (PRDX1), has been observed and confirmed. Anti-RCC evaluation *in vitro* and *in vivo* confirmed that the piericidins behave as potent anti-RCC agents.

2. Results

2.1. Natural piericidins and their activities against renal cancer cells

In order to explore natural piericidins compounds, chemical dereplication by HPLC/MS was performed to screen the strains with piericidins in marine *Streptomyces* strains in our lab. The HPLC/MS analysis uncovered abundant and divers piericidin glycosides in the strain *Streptomyces psammoticus* SCSIO NS126 (Supporting information, **Figure S1**), an actinomycete strain isolated from a mangrove sediment sample collected from the Pearl River estuary to South China Sea. Chemical study of the culture (60 L for liquid fermentation) extract of strain SCSIO NS126 provided 27 natural piericidins (**Figure 1**).

Among the natural piericidins obtained, seventeen (**2**–**5**, **12**, **13**, **15**, **17**–**26**) were identified as new natural products, by extensive NMR and HRMS analyses, including their configurations as defined by NOESY data, coupling constant analysis, and ECD comparisons, along with their biosynthesis taken into consideration.

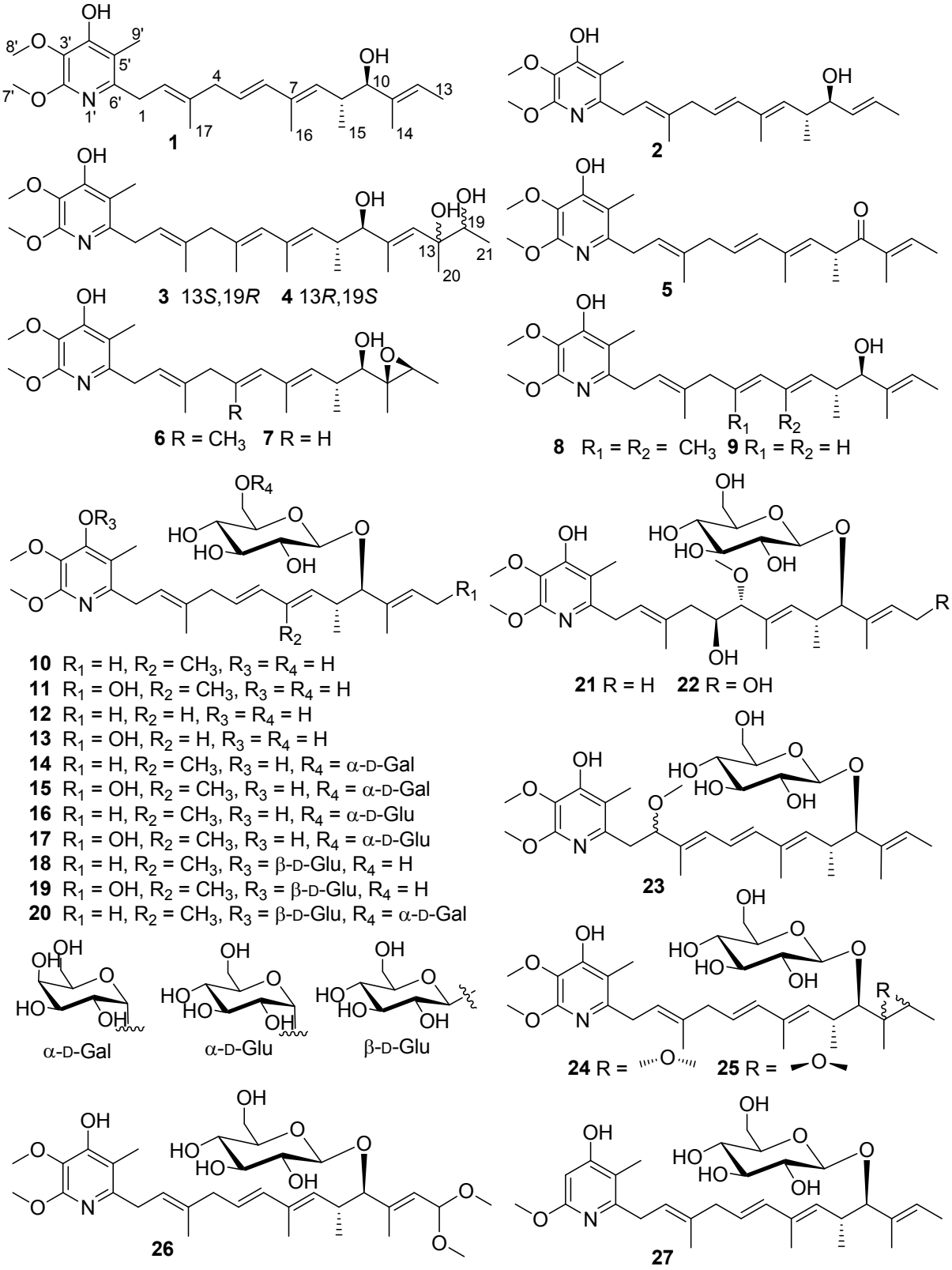

Figure 1. Structures of the piericidins obtained from the *Streptomyces* strain SCSIO NS126.

Comparison of the NMR date of **2** with those of piericidin A (**1**) indicated that the only difference was the absence of the 14-methyl group in **2**, which was confirmed by the HMBC and COSY correlations. Compound **2** was identified as 11-demethyl-piericidin A (**2**). Two hydroxyl groups on C-13 and C-19 were confirmed in the structures of **3** and **4**, and their absolute configurations were determined by calculated and experimental ECD curves (**Figure S9**). Compound **5** was identified as the same structure and same absolute configuration (9*R*) as synthetic C-10 ketone piericidin A, [9] and obtained as a natural product firstly here. Compound **12** was suggested to be a glycoside of 7-demethylpiericidin A1 (**9**), and 10-*O*-*β*-D-glucoside linkage was determined by the NMR analysis, as well as the acid hydrolysis. Compound **13** was characterized as 7-demethyl-13-hydroxyglucopiericidin A (**13**). Compounds **14-19** were showed to be diglycosides of piericidin. Compounds **14** and **16** were characterized as piericidin A 10-*O*-α-D-galactose (1→6)-β-D-glucoside (**14**) and piericidin A 10-*O*-*α*-D-glucose (1→6)-*β*-D-glucoside (**16**), respectively, by acid hydrolysis and NMR analysis. The additional *β*-D-glucose group of **18** was linked on OH-4′ of the pyridine ring, so the structure was characterized as 4′-*O*-*β*-D-glucose glucopiericidin A (**18**). Compounds **15**, **17** and **19** were showed to be 13-hydroxy derivatives of **14**, **16** and **18**, respectively. Compound **20** was indicated as a triglycoside of piericidin by HR-ESIMS and NMR date, and characterized as 4′-*O*-*β*-D-glucose piericidin A 10-*O*-*α*-D-glucose (1→6)-*β*-D-glucoside (**20**). In the structure of **21**, C-5/C-6 double bond was replaced by 5-hydroxy-6-hydroxymethyl group, with their configurations determined by coupling constant and NOESY correlation. Compound **22**, the 13-hydroxy derivatives of **21**, was characterized as 5-hydroxy-6-hydroxymethyl-13-hydroxyglucopiericidin A (**22**). The conventional C-2/C-3 double bond was moved to C-3/C-4 in glycoside **23**, and an additional hydroxymethyl was linked on C-2. Compound **23** was characterized as 2-hydroxymethyl-*Δ*3, 4-

glucopiericidin A (**23**), with the absolute configuration of C-2 remained to be defined. Glycosides **24** and **25** have the same planer structure, including the C-11/C-12 epoxy ring. The configurations of the C-11/C-12 in **24** and **25** were determined to be 11*S*,12*R* and 11*R*,12*S*, respectively, by NOESY and ECD analysis. The chemical shifts of CH-13 and HR-ESIMS data suggested two methoxy groups linked on C-13 in **26**, which were supported by HMBC correlations. So, **26** was characterized as 13-dimethoxy glucopiericidin A (**26**). The other reported compounds were identified by comparison of their spectroscopic data with those in the literature. The details of the structure elucidation were supported in the **Supporting information**.

From the genome sequence of this actinomycete strain, we identified the biosynthetic gene cluster of PA (**1**), which displays the same genetic organization as that in *Streptomyces piomogeues* (**Table S7**), [10,11] together with several glycosyltransferases. Diverse oxygenated piericidin derivatives, such as the seven 13-hydroxy piericidin glycosides and several derivatives with 5,6-dihydroxy, 13,19-dihydroxy or those with the C-11/C-12 epoxide ring, suggest that there are additional oxygenases taking part in the biosynthesis of these piericidin derivatives. The 13,19-dihydroxy functionality (in **3** and **4**), 5,6-dihydroxy functionality (in **21** and **22**), and also the 2-hydroxymethyl group (in **23**) are proposed to be formed by epoxidation and ring opening, the latter of which is followed by dehydration. Eighteen glycosides (**10**–**27**), composed of eleven monoglycosides, six diglycosides and one triglycoside, expand the diversity of natural piericidin glycosides. Diglycosides of piericidin have been rarely reported, and the triglycoside (**20**) here is the first piericidin triglycoside reported from nature.

Most of the piericidins were evaluated for their cytotoxicities against three renal carcinoma cell lines, ACHN, OS-RC-2, and 786-O, as well as a normal renal cell line, HK-2 (**Table 1**).

Most of the piericidins showed strong to moderate cytotoxicities toward ACHN, and several analogs, such as PA (**1**), glucopiericidin A (GPA, **10**) and **12**, showed significant activities with IC_{50} values less than 1 μM (**Table 1**). OS-RC-2, 786-O, and HK-2 cells were not as sensitive as ACHN to most of the piericidins.

Table 1. The cytotoxicity of the piericidins (IC_{50}, μM).

	ACHN	OS-RC-2	786-O	HK-2	shPRDX1 ACHN
1	0.40	5.2	30	>100	1.6
2	4.1	11	>100	–	11
3	2.4	5.3	>100	44	8.2
4	3.8	4.1	>100	63	13
5	>100	22	>100	–	>100
6	>100	22	>100	>100	>100
8	14	17	50	45	68
10	0.21	>100	>100	>100	0.96
11	7.21	>100	>100	>100	–
12	0.31	2.6	0.99	–	–
13	2.5	79	28	–	–
14	4.5	>100	>100	>100	9.0
15	>100	>100	>100	>100	–
16	21	>100	>100	>100	–
17	23	>100	>100	>100	58
18	28	>100	>100	1.1	–
21	2.4	>100	>100	–	–
22	60	>100	>100	–	–
23	1.7	60	28	–	–
24	2.8	30	19	–	–
27	3.8	14	15	–	–
Sora	3.3	14	13	2.6	–

Sora: Sorafenib; – Unrecorded.

2.2. PA/GPA up-regulates PRDX1 that is lower in ccRCC

To investigate the underlying molecular mechanisms of PA (**1**) on ACHN cells, we analyzed transcriptome alterations using high-depth next generation sequencing with an Illumina HiSeq 4000. In total, more than 291 million stranded 150 basepairs (bp) paired-end reads were sequenced from 3 groups of ACHN cells treated with two doses of PA (25 and 50 nM) for 24 hours along with untreated cells. All mRNA sequencing data has been submitted to the GEO repository (GSE116158) (**Table S1**). Next, DEseq was used to identify the statistically significant differentially expressed genes (DEGs) for the pairwise comparisons between these three groups respectively. Among 17,847 detected unigenes, 6035 genes (2862 up regulated and 3173 down regulated) had significantly altered expression in cells treated with low dose PA, while more DEGs (8,889 genes total, 4305 up regulated and 4584 down regulated) were identified in high dose PA treatment (**Figure 2**A, **Table S2**). Given the significant effect of high dose PA treatment, an intersection of DEGs in two experimental groups was performed to locate the key genes affected. Then, KEGG pathway enrichment analysis, according to 1066 DEGs from the intersection of three groups (**Table S3**), was employed to identify the biological characterization of the significantly regulated genes. The results showed that the regulated genes were involved in endoplasmic reticulum, pathways in cancer, HIF-1 signalling pathway, and renal carcinoma pathways (**Figure 2**C, **Table S4**). Then supervised weighted correlation network analysis (sWGCNA) was employed to define hub genes and the relationship among the selected DEGs from those pathways (**Figure S4**).

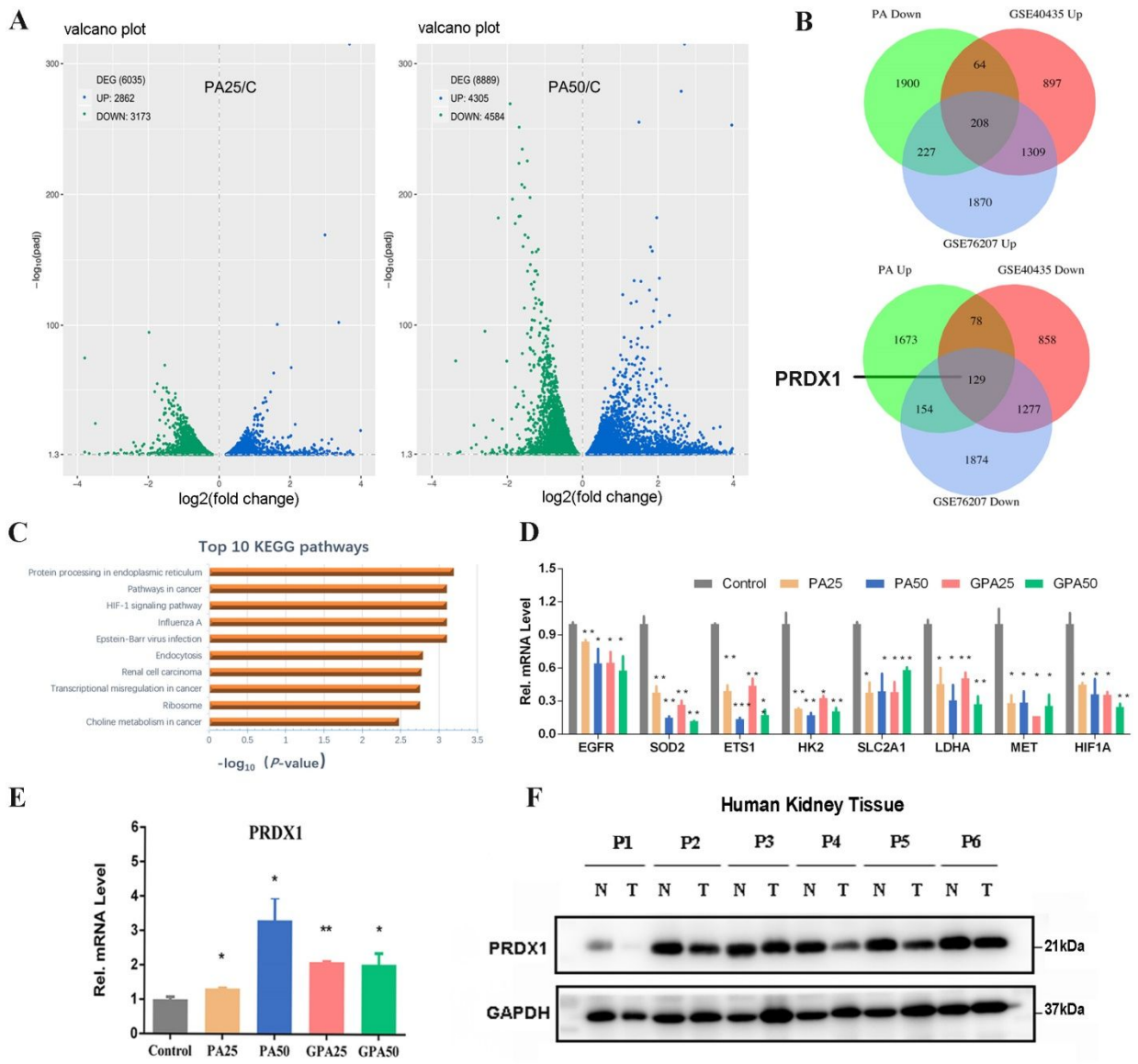

Figure 2. Transcriptome analysis of gene expression profile in ACHN cells treated with PA. A) Volcano Plot: showed numbers of DEGs (FDR < 0.05 according to edgeR). B) The intersection of DEGs (the statistical criteria using fold change > 1.5 and FDR < 0.05) effected by PA and those DEGs from pairs of ccRCC tumours and adjacent non-tumour renal tissues from GSE40435 and GSE76207. C) KEGG pathways enrichment analysis. The bars represent the enrichment scores, -log10 (*P* value). D) PA (25 and 50 nM) and GPA (25 and 50 nM) reduced the activation of key genes in ACHN cells. E) mRNA level of PRDX1 in ACHN cells after treatment of PA/GPA. F) Immunoblot analysis of PRDX1 protein of extracts of paired tumour (T) versus adjacent non-tumour (N) samples from 6 human ccRCC patients.

Consequently, multiple interaction genes (*EGFR, SOS2, ETS1 and HK2, SLC2A1, LDHA, MET, HIF1A*, etc.,), among the above signalling pathways were chosen to be certificated treated with PA and GPA (25 and 50 nM) in ACHN cells by RT-PCR (**Figure 2**D). GPA (**10**), with similar inhibitory activity towards ACHN as PA, is the glycoside of PA (**1**). As expected, PA and GPA could both reduce the activation of those key genes. Thus, there are reasons to believe that PA and GPA exert their tumour-inhibition activity through the same pathway. To further clarify the potential molecular targets, we examined the intersection of DEGs (the statistical criteria using fold change ≥ 1.5 and FDR < 0.05) affected by PA and those DEGs between pairs of clear cell renal cell carcinoma (ccRCC) tumour and the adjacent non-tumour renal tissues in GEO database (GSE40435 and GSE76207) (**Figure 2**B). There were 129 common genes up-regulated in the PA treatment group but down-regulated in the ccRCC tumour tissues compared to the adjacent non-tumour renal tissues, including *PRDX1* (**Figure 2**B). RT-PCR was employed to certify the up-regulation of PRDX1 in ACHN cells after treatment of PA/GPA (**Figure 2**E).

As a redox-regulating protein belongs to the ubiquitous PRDXs family, PRDX1 was implicated in regulating cell proliferation, differentiation, and apoptosis.[12] All peroxiredoxins have been shown to have altered expression in human cancer, being up-regulated in breast cancer, oesophageal cancer, and lung cancer, but down-regulated in thyroid cancer as a tumour suppressor.[13,14] PRDX1 protein was decreased in ccRCC as compared to adjacent normal renal tissue. [15] Remarkably, we make the same findings of the lower PRDX1 protein levels in six ccRCC tumour samples (**Figure 2**F, **Table S10**). Along with the analysis of different GEO datasets, it's reasonable to believe that the mRNA and protein level of PRDX1 are lower in renal tumour tissues, and PRDX1 could be considered as a potential target in RCC. However, the mechanism of PRDX1 as an anti-RCC target still needs to be further explored.

2.3. PA/GPA induce cell apoptosis through increasing PRDX1 and reducing ROS

PRDX1 was firstly reported as an antioxidant enzyme because of its functions to eliminate peroxide *in vivo* and regulate reactive oxygen species (ROS).[13] Aggressive cancer cells depend on elevated intracellular levels of ROS to proliferate, self-renew, metastasize, etc. These aggressive cancers maintain high basal levels of ROS compared to normal cells.[16] With a high ROS level and low PRDX1 expression, RCC becomes less sensitive to radiation and chemotherapy. Thus, ROS elimination played a vital role in RCC treatment. To explore the molecular mechanisms of piericidins (PA/GPA) on ACHN cells, clarifying the relationship between PRDX1 and ROS levels in RCC is crucial.

To further illustrate the mechanism by which PRDX1 exerts its tumour-suppressing effect, we created knockdown PRDX1 ACHN cells (PRDX1-Kd) using lentivirus PRDX1 shRNA (shPRDX1) to speculate on the role of ROS (**Figure 3**B, **Figure S5**). As a result, the knockdown of PRDX1 raised ROS levels compared to normal ACHN cells (**Figure 3**C1). ROS reduction in normal ACHN cells was observed when treated with PA/GPA (25 and 50 nM) (**Figure 3**C2). Notably, knockdown of PRDX1 eliminated these effects, which indicated that PRDX1 was the target of PA/GPA (**Figure 3**C3). By decreasing ROS levels, PA showed significant proliferation suppression as well as inducing apoptosis of ACHN cells (**Figure 3**A1/A2). In addition, the cytotoxic IC_{50} values of PA/GPA against shPRDX1 ACHN cells were almost 4-fold higher than normal ACHN cells with slight toxicity towards HK2 cell (**Table 1**). These results indicated that PA/GPA targets PRDX1 mainly increasing mRNA and protein levels rather than improving the antioxidant activity (**Figure S6**).

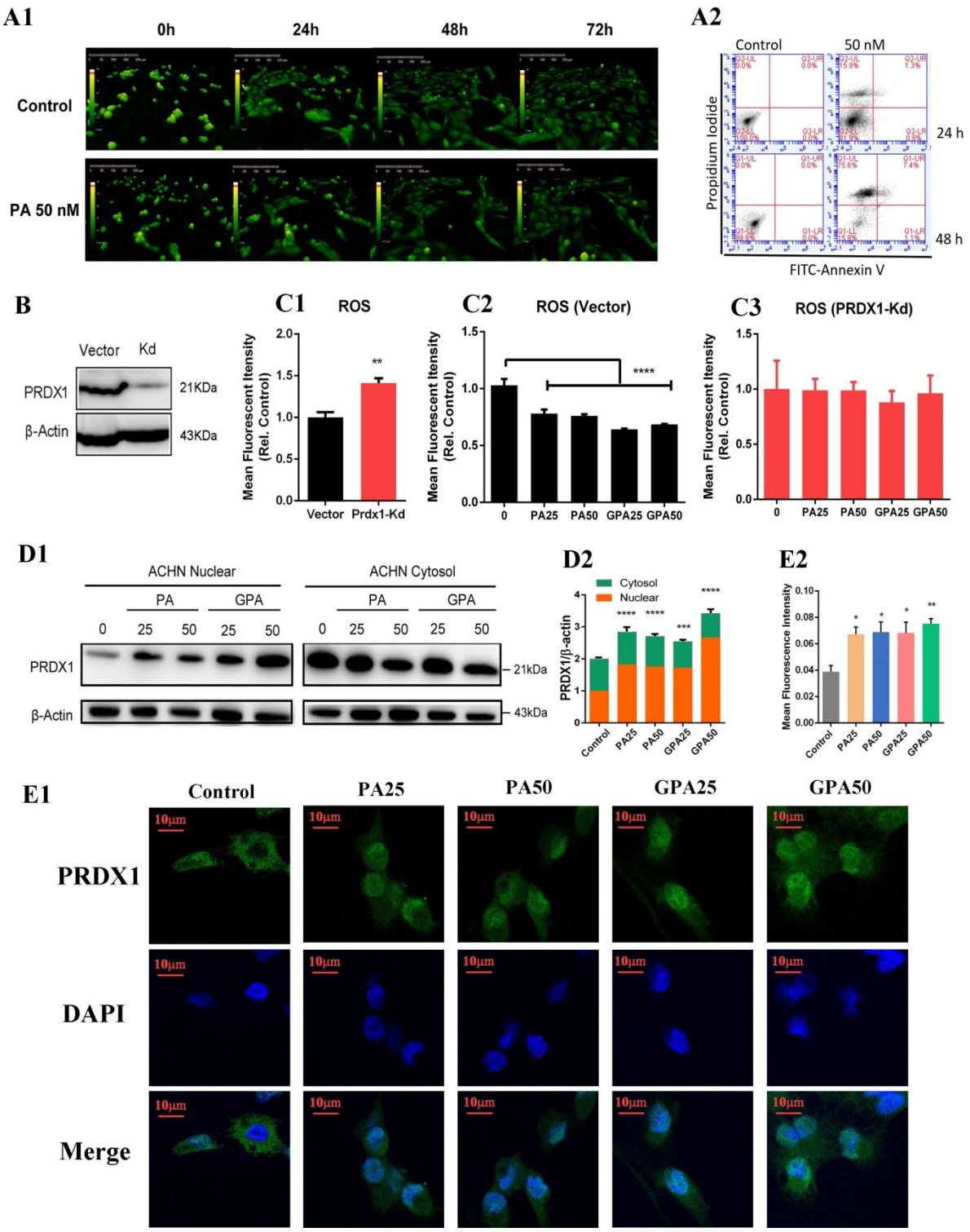

Figure 3. PA/GPA inhibits cell proliferation and induced cell apoptosis through increasing PRDX1 and reducing ROS in ACHN. A1) Phase holographic imaging of ACHN cells treated with PA (50 nM) for

72h. A2) Annexin V/PI staining and flow cytometry showed the percentages of apoptosis in ACHN cells treated with PA (50 nM). B) Immunoblot analysis of PRDX1 protein in the normal ACHN cells and PRDX1-Kd ACHN cells; C1) The intracellular ROS detection with flow cytometer in the normal ACHN cells and PRDX1-Kd ACHN cells. C2) The intracellular ROS detection in the normal ACHN cell treated by PA/GPA (25 and 50 nM) in 24h; C3) The intracellular ROS detection in the PRDX1-Kd ACHN cell treated by PA/GPA (25 and 50 nM) in 24h. D1) Immunoblot analysis of PRDX1 protein in nuclear and cytosol extracts of ACHN cell treated with PA/GPA (25 and 50 nM). D2) Fold change of protein expression (PRDX1/β-Actin). E1) Representative images for immunofluorescent staining of ACHN treated with PA/GPA (25 and 50 nM) after co-incubating for 24h. PRDX1 (green), nucleus (blue), n = 9. Scale bar = 10 μm. E2) Mean fluorescence intensity of ACHN cell treated with PA/GPA (25 and 50 nM) in 24h. All data represent mean ± SD. Statistical significance was determined using Student's *t* test or one-way ANOVA with Tukey's post-hoc test. *$p < 0.05$, **$p < 0.01$, ***$p < 0.005$, ****$p < 0.001$.

Not only serving as antioxidant enzyme, PRDX1 can also act as a molecular chaperone with the ability to modulate actions of numerous molecules or as a regulator of transcription. [17,18] PRDX1 could directly bind with nuclear transcriptional factors and modulate gene expression such as c-Myc and NF-κB. [19] So, we further investigated the PRDX1 protein level in nuclear and cytosol of ACHN cell. Along with increasing total PRDX1, obvious translocation of PRDX1 towards nucleus was also observed, indicated that PA/GPA not only raised the expression of mRNA and protein of PRDX1 but also forced it into nucleus (**Figure 3**D/E). Some studies have shown that PRDX1 in the nucleus leads to inhibition of NF-κB activation, a typical oncogene involved in most cancers. [20] These data further suggested that the protein level of PRDX1, but not antioxidant activity, is critical in regulating the ROS level and the inactivation of NF-κB.

2.4. Docking analysis of PA/GPA with PRDX1

The interconversion between the dimeric and decameric forms of PRDX1 is influenced by redox state or protein concentration, and the dimeric form is preferred for translocation into the nucleus.[21] In order to further understand the interaction between PA/GPA and the potential target, especially regulatory mechanisms of dimer-oligomer interconversion of PRDX1, Induce-fit module in the Schrödinger suite was employed to perform the *in silico* molecular docking analysis. The chains a, b, c, and d, as a dimer-dimer interface unit, from the reduced decameric form of PRDX1 (PDB entry 2Z9S, **Figure S7**) was used as the receptor structure (**Figure 4**A1). Since the redox status CYS83 might influence the oligomeric structure and consequently the functions of PRDX1 in regulating the peroxidase and chaperone activities,[22] it was selected as Trim residue and the center of active pocket, which composed of the PHE48, TRP87 from the dimer-dimer interface.[21] As the results, the pyridine ring of PA/GPA played a key role to form a π-π stacking interaction with PHE48. Moreover, the π cation interaction was formed between pyridine ring and LYS192, and hydrophobic interaction was formed between side chain and dimer-dimer interface (**Figure 4**A2/A3). The hydroxyls at side chain and pyridine ring formed hydrogen bonds with the residues GLN94, GLY95 in chain a and LYS192 in chain c, respectively. It is suggested that those interactions inhibit the formation of the oligomeric state of PRDX1 and forced the active dimer into the nucleus, which consistent with the experimental findings about the increase of PRDX1 in nucleus (**Figure 3**D/E).

The docking study showed that the interactions between PA/GPA and single dimer (docking scores about –6) of PRDX1 were much weaker than with dimer-dimer interface (docking scores about –10). The dissociation equilibrium constants (K_D) of PRDX1 protein with PA (2.61×10^{-6} M) and GPA (1.83×10^{-6} M), measured by a surface plasmon resonance (SPR) assay (**Figure 4B**), revealed the affinity interaction between PA/GPA and PRDX1 protein (**Figure 4**B1/B2).

Therefore, it is suggested that, not only combined with the PRDX1, PA/GPA could force PRDX1 translocate into nucleus is also proposed to be a key factor for the anti-RCC procedure of PA/GPA.

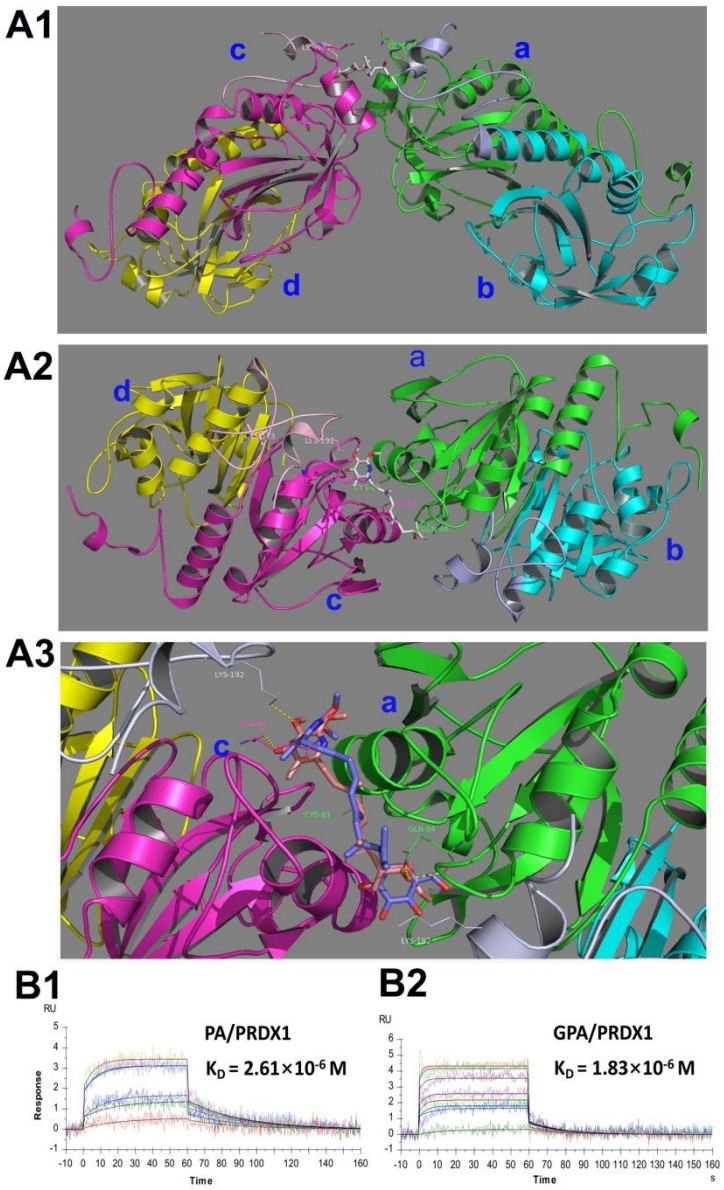

Figure 4. Molecular docking and SPR analysis of PA/GPA with PRDX1. A1) Dimer-dimer interface region (PDB entry 2Z9S) was used as the receptor structure. Each chain of monomers is shown in different colors. Chains a, b as a dimer and chains c, d as another dimer. CYS83-CYS83 disulfide bridge is located between chains a and c. A2) Binding sites and the details of the predicted binding mode of PA

in dimer-dimer interface of PRDX1 (2Z9S), 90° rotation from A1. A3) Binding sites and the details of the predicted binding mode of GPA in dimer-dimer interface of PRDX1 (2Z9S) The contact residues are shown and labelled by type and number. B) The affinity activities of PA (B1) and GPA (B2) to PRDX1 protein was analyzed using the SPR assay.

2.5. Anti-tumor efficacy of PA and GPA in nude mice bearing ACHN xenografts

Since PA and GPA showed significant inhibitory effects against ACHN *in vitro*, the *in vivo* their anti-cancer therapeutic potential were further investigated. Nude mice bearing ACHN tumor xenografts were divided into four groups (control group with only PBS injection, PA and GPA groups with both 0.8 mg/kg, sorafenib group with 50 mg/kg),[23] and PA and GPA were administered through intraperitoneal (ip) injection daily for three weeks. The treatment outcome was assessed by monitoring relative tumor volumes and weights of the mice, and tumor tissue ablation was also evaluated by HE (haematoxylin and eosin) staining and TUNEL (terminal deoxynucleotidyl transferase (TdT)-mediated dUTP nick end labelling) staining on tissue sections.

As shown in **Figure 5**, administration of PA or GPA significantly reduced the final tumor weight of the mice (mean 0.28 g to PA, and mean 0.23 g to GPA) as compared to the control group (mean 0.55 g), basically matching the tumor volume curves (**Figure 5**A/B). All the mice in the treatment groups survived more than three weeks, the mice body weights of PA and GPA groups did not decrease as observed in the sorafenib group (**Figure 5**B). PA and GPA showed significant anti-tumor efficacy in nude mice bearing ACHN xenografts with low effective dose and without serious side effects.

After administration of PA and GPA for 21 days, the mRNA and protein expression of PRDX1 in tumor tissues increased (**Figure 5**C), consistent with the results *in vitro*. In addition,

TUNEL staining indicated by green colour staining and HE staining results in tumor tissues treated with PA or GPA further demonstrated the inhibition of tumor growth (**Figure 5**D).

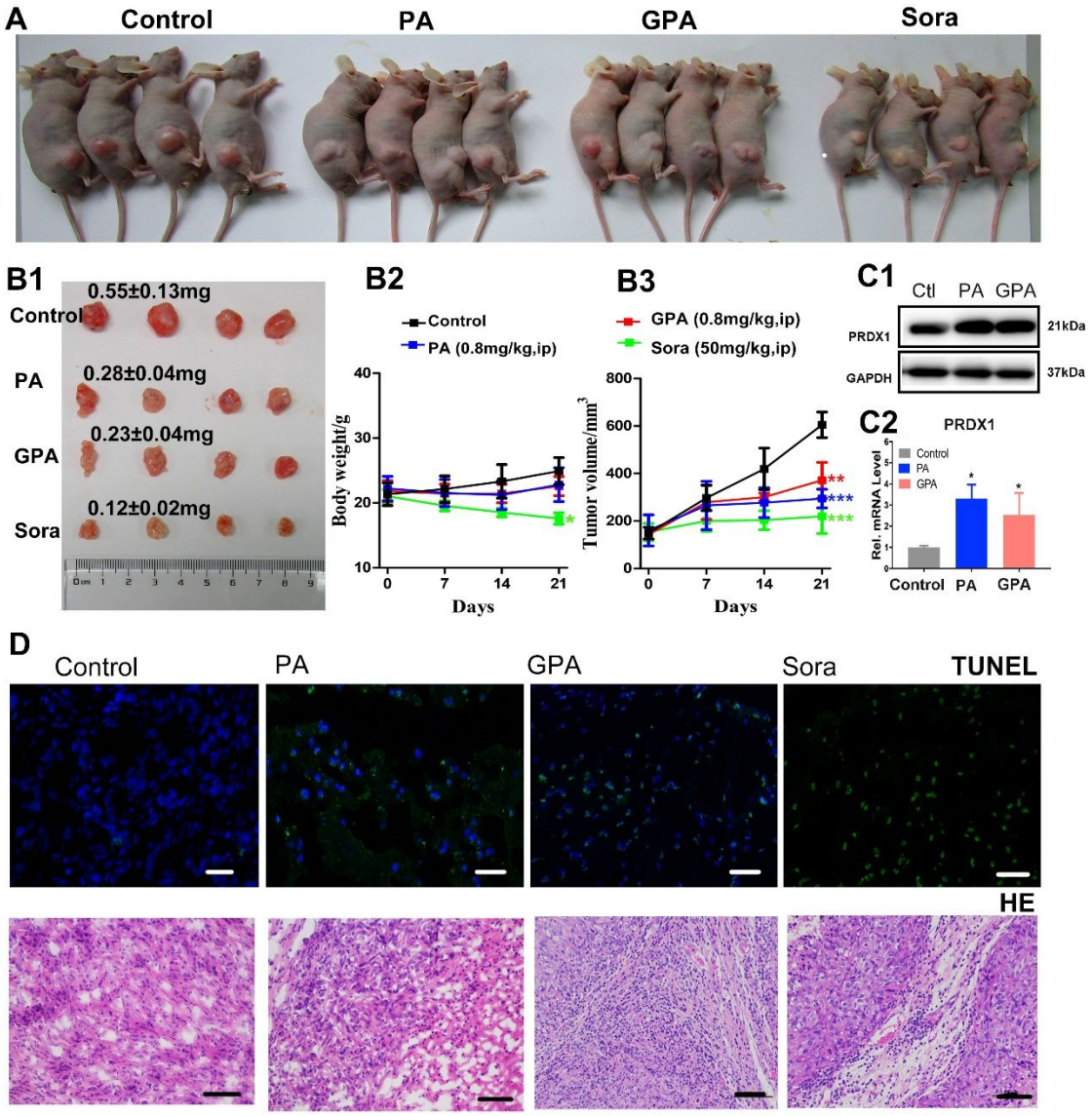

Figure 5. PA and GPA show anti-tumor efficacy in nude mice bearing ACHN xenografts. A) Images of mice bearing ACHN xenografts and injected ip once a day at day 21 post injection. B) Images of tumor (B1) and progression of body weights (B2) and tumor volumes (B3) in mice during 21 days treatment; n = 4, ± SE. C) Immunoblot analysis of PRDX1 protein in tumor tissues after 21 days treatment with saline,

PA and GPA. D) TUNEL and HE staining of tumor sections after treatment, respectively. Scale bar, 100 μm.

3. Discussion

In this study, twenty seven natural piericidins were obtained from a *Streptomyces* strain isolated from the mangrove sediments. Seventeen were identified as new natural products, including thirteen new piericidin glycosides. This work has extended the chemical diversity of this family, although several piericidin glycosides have been detected and structurally predicted *in situ* in the symbiotic *Streptomyces* strains of beewolf host species reported recently. [24] The availability of these diverse piericidin natural products creates an opportunity to fully understand the importance of these compounds. Although the cytotoxicity of the piericidins are commonly reported, the potential to treat renal cancer or related cancer cells was not realized. As one of the high incidence cancers with poor prognosis, our findings highlight the inhibition activity of piericidins against renal cancer *in vitro* and *in vivo*.

Cancer cells rely on the signaling capabilities of ROS for cell migration, proliferation, and survival. [25] Studies have found that persistent high level of ROS can act as mitogenic or genotoxic signals, inhibiting the sensitivity of radiotherapy and chemotherapy in cancer cells. [26,27] As a member of the ubiquitous family of redox-regulating proteins, PRDX1 is reported to potentially eliminate various ROS. The dimeric form is considered to be the active and functional form of PRDX1, and is preferred for translocation into the nucleus. [21] PRDX1 can directly combine with some transcription factors in the nucleus such as c-Myc and NF-κB, affecting their bioactivities upon gene regulation, which in turn induces or suppresses cell death. Using bioinformatics analysis of clinical samples, ccRCC is thought to be a malignant tumor with lower PRDX1 level. Remarkably, piericidins (PA/GPA) target PRDX1, increasing the

mRNA and protein levels of PRDX1, which reduces ROS levels in ACHN cells along with obvious cell apoptosis induction and proliferation inhibition. Besides, PA/GPA can interact directly with PRDX1 protein and increase the nucleus co-localization, thereby inhibiting the activation of key genes in the renal caner pathway. Moreover, our study revealed that ACHN cells were less sensitive to piericidins when PRDX1 was down-regulated. Therefore, our direct evidence shows that PA/GPA targets PRDX1 and reduces ROS in ACHN cells.

In those twenty seven natural piericidins obtained in this study, PA and GPA were investigated with their molecular mechanisms on renal carcinoma cells, as well as the *in vivo* anti-cancer evaluation. PA and GPA were being chosen as representative molecules of piericidin aglycones and glycosides, respectively, because of their relative high yield in the *Streptomyces* strain and their significant inhibitory ability against ACHN cells *in vitro*. There were no obvious differences between the piericidin glycosides and aglycones in the cytotoxicity against ACHN cells. Moreover, the nearly indistinguishable anti-tumor effects *in vivo* between PA and GPA in our study suggest that, the same metabolic substances might contribute to the efficacy after drug metabolism *in vivo*. However, the up-regulation of PRDX1 protein expression by GPA in the nucleus of ACHN cells appears stronger than that of PA (**Figure 3**D). And the affinity interaction measured by SPR test also showed glycoside GPA bound more effectively than the aglycone PA with PRDX1 (**Figure 4B**). In this study, we found that PRDX1 could be used as an important new target for anti-RCC agents, and piericidins such as PA and GPA could be considered as lead compounds targeting PRDX1.

4. Conclusion

In conclusion, twenty seven natural piericidins were discovered by cultivation of a marine-derived *Streptomyces* strain, and their potential in anti-RCC was demonstrated. The low effective

dose and relative safety of PA and GPA *in vivo* suggests these maybe developed as new anti-RCC agents. The site of action of these agents targeting PRDX1, may improve upon the limitations of mechanisms of existing targeted drugs for the treatment of RCC. Although more investigations are needed, our current studies reveal that piericidins could conceivably provide a novel scaffold for further development of potent and mechanistically-novel anti-RCC agents.

5. Experimental Section

5.1 Chemistry. IR spectra were measured on an IR Affinity-1 spectrometer (Shimadzu). Optical rotations were performed on a PerkinElmer 341 polarimeter. ECD spectra were measured with a Chirascan circular dichroism spectrometer (Applied Photophysics). The NMR spectra including 1D and 2D NMR were recorded on Bruker AC 500/700 MHz spectrometers. HR-ESIMS were determined with a Bruker maXis Q-TOF in positive/negative ion mode. Column chromatography was performed on silica gel (200−300, 300−400 mesh) and Sephadex LH-20 (Amersham Biosciences), respectively. All solvents used were of analytical grade (Tianjin Fuyu Chemical and Industry Factory). The semipreparative HPLC was performed on an HPLC (Hitachi-L2130, diode array detector, Hitachi L-2455, Tokyo, Japan) using a Phenomenex ODS column (250 mm × 10.0 mm i.d., 5 μm; Phenomenex, USA).

5.2 Strain Material. The strain SCSIO NS126 was isolated from a mangrove sediment sample collected from the Pearl River estuary (E 113°33′11.15″, N22°53′40.16″) to South China Sea in May 2015, by incubation at 28 °C for two weeks on ISP-2 medium (yeast extract 4 g, malt extract 4 g, glucose 4 g, crude sea salt 30 g, agar powder 20 g, distilled water 1000 mL, pH, 7.2-7.4). The strain was identified as a *Streptomyces psammoticus* specie, by the 16S rRNA gene sequence analysis (**Table S8**). It was deposited at the China Center for Type Culture Collection (Wuhan) as CCTCC M2017099 (*Streptomyces psammoticus* SCSIO NS126).

5.3 Fermentation and Extraction. The strain SCSIO NS126 was fermented for 60 L. A few loop of cells of the strains were inoculated into a 250 mL Erlenmeyer flask containing 50 mL of seed medium (mannitol 1 g, soya peptone 0.5 g, soya-bean oil 0.125 g, K_2HPO_3 0.02 g, pH 7.0, 50 mL distilled water), and then cultivated on a rotary shaker at 120 rpm, 28 °C for 48 h as seed culture. Then, 2 mL of seed culture was inoculated into a 500 mL Erlenmeyer flask containing 100 mL media (cotton seed meal 2.5 g, soluble starch 1 g, glucose 1 g, yeast extract 0.3 g, $CaCO_3$ 0.5 g, sea salt, 0.2 g; in 100 mL distilled water, pH 7.2). After cultivation on a rotary shaker at 180 rpm and 28 °C for 120 h, each bacterial culture broth was broken with ultrasonic treatment apparatus for 10 min. Then culture broth was extracted with an equal volume of ethyl acetate three times. The organic extract was then concentrated under vacuum to afford the crude extract.

5.4 Compounds Isolation. The extract of strain SCSIO NS126 (38.2 g) was chromatographed on silica gel to give eight fractions (Frs.1–8). With the guide of HPLC analysis, Frs.2 and Frs.3 were combined and further purified by silica gel to obtain pure compound **1** (230 mg), **2** (13 mg), **5** (16 mg), **6** (12 mg), **8** (14 mg), and **9** (3.7 mg). Frs.4 was further purified by semipreparative HPLC to get compound **3** (0.7 mg) and **4** (0.8 mg) and **7** (2.5 mg). Frs.5 was further purified by semipreparative HPLC to get **10** (78 mg), **12** (2.9 mg), **23** (1.9 mg), **26** (1.1 mg) and **27** (2.1 mg). The compound **10** (250 mg) with the highest content was purified and obtained by semipreparative HPLC from Frs.6, together with **14** (6.5 mg), **16** (3.2 mg), **18** (2.5 mg), **21** (1.8 mg), **24** (1.6 mg) and **25** (0.6 mg). Frs.7 was also purified by semi-preparative HPLC to get **11** (28 mg) **13** (1.8 mg), **15** (6.9 mg), **17** (4.1 mg), **19** (1.5 mg), **20** (1.5 mg), and **22** (1.9 mg). All obtained compounds were determined to have ≥95% purity by analytical HPLC.

11-Demethyl-piericidin A (**2**). Pale yellow oil; IR (film) ν_{max} 3335, 2945, 1449, 1020, 667 cm^{-1}; ^{1}H and ^{13}C NMR data, Tables **S2-1** and **S2-2**; HR-ESIMS *m/z* 402.2649 $[M+H]^+$ (calcd for $C_{24}H_{36}NO_4^+$, 402.2639).

(2*E*,5*E*,7*E*,11*E*,9*R*,10*R*,13*S*,19*R*)-13,19-Dihydroxyl-IT-143-A (**3**). Pale yellow oil; IR (film) ν_{max} 3335, 2945, 1449, 1020, 667 cm^{-1}; ^{1}H and ^{13}C NMR data, Tables **S2-1** and **S2-2**; HR-ESIMS *m/z* 504.3332 $[M+H]^+$ (calcd for $C_{29}H_{46}NO_6^+$, 504.3320).

(2*E*,5*E*,7*E*,11*E*,9*R*,10*R*,13*R*,19*S*)-13,19-Dihydroxyl-IT-143-A (**4**). Pale yellow oil; IR (film) ν_{max} 3329, 2945, 1446, 1018, 667 cm^{-1}; ^{1}H and ^{13}C NMR data, Tables **S2-1** and **S2-2**; HR-ESIMS *m/z* 504.3320 $[M+H]^+$ (calcd for $C_{29}H_{46}NO_6^+$, 504.3320).

10-Ketone piericidin A (**5**). Clear oil; [α]20 D – 5.5, *c* 0.2, $CHCl_3$; IR (film) ν_{max} 3332, 2945, 1472, 1018, 667 cm^{-1}; ^{1}H and ^{13}C NMR data, Tables **S2-1** and **S2-2**; HR-ESIMS *m/z* 414.2657 $[M+H]^+$ (calcd for $C_{25}H_{36}NO_4^+$, 414.2639).

7-Demethylglucopiericidin A (**12**). Pale yellow oil; IR (film) ν_{max} 3420, 2928, 1472, 1456, 1125, 1016, 652 cm^{-1}; ^{1}H and ^{13}C NMR data, Tables **S2-3** and **S2-5**; HR-ESIMS *m/z* 564.3185 $[M+H]^+$ (calcd for $C_{30}H_{46}NO_9^+$, 564.3167).

7-Demethyl-13-hydroxyglucopiericidin A (**13**). Pale yellow oil; IR (film) ν_{max} 3302, 2930, 1585, 1464, 1412, 1125, 1022, 650 cm^{-1}; ^{1}H and ^{13}C NMR data, Tables **S2-3** and **S2-5**; HR-ESIMS *m/z* 580.3126 $[M+H]^+$ (calcd for $C_{30}H_{46}NO_{10}^+$, 580.3116).

13-Hydroxypiericidin A 10-*O*-*α*-D-galactose (1→6)-*β*-D-glucoside (**15**). Pale yellow oil; IR (film) ν_{max} 3319, 2930, 1650, 1412, 1126, 1022, 824, 764, 667 cm^{-1}; ^{1}H and ^{13}C NMR data, Tables **S2-3** and **S2-5**; HR-ESIMS *m/z* 754.3646 $[M – H]^-$ (calcd for $C_{37}H_{56}NO_{15}^-$, 754.3655).

13-Hydroxypiericidin A 10-*O*-*α*-D-glucose (1→6)-*β*-D-glucoside (**17**). Pale yellow oil; IR (film) ν_{max} 3358, 2920, 1585, 1412, 1125, 1022, 824, 764, 667 cm^{-1}; ^{1}H and ^{13}C NMR data, Tables **S2-3** and **S2-5**; HR-ESIMS *m/z* 754.3660 $[M – H]^-$ (calcd for $C_{37}H_{56}NO_{15}^-$, 754.3655).

4′-*O*-*β*-D-Glucose glucopiericidin A (**18**). Pale yellow oil; IR (film) ν_{max} 3366, 2920, 1582, 1404, 1047, 669 cm^{-1}; ^{1}H and ^{13}C NMR data, Tables **S2-3** and **S2-5**; HR-ESIMS *m/z* 738.3684 $[M – H]^-$ (calcd for $C_{37}H_{56}NO_{14}^-$, 738.3706).

4′-*O*-*β*-D-Glucose 13-hydroxyglucopiericidin A (**19**). Pale yellow oil; IR (film) ν_{max} 3292, 2943, 1456, 1404, 1020, 660 cm^{-1}; ^{1}H and ^{13}C NMR data, Tables **S2-3** and **S2-5**; HR-ESIMS *m/z* 756.3829 $[M + H]^+$ (calcd for $C_{37}H_{58}NO_{15}^+$, 756.3801).

4′-*O*-*β*-D-Glucose piericidin A 10-*O*-*α*-D-glucose (1→6)-*β*-D-glucoside (**20**). Pale yellow oil; IR (film) ν_{max} 3342, 2930, 1568, 1456, 1018, 650 cm^{-1}; ^{1}H and ^{13}C NMR data, Tables **S2-4** and **S2-5**; HR-ESIMS *m/z* 902.4390 $[M + H]^+$ (calcd for $C_{43}H_{68}NO_{19}^+$, 902.4380).

5-Hydroxy-6-hydroxymethyl glucopiericidin A (**21**). Pale yellow oil; IR (film) ν_{max} 3356, 2916, 1568, 1471, 1412, 1016, 667 cm^{-1}; ^{1}H and ^{13}C NMR data, Tables **S2-4** and **S2-5**; HR-ESIMS *m/z* 626.3543 $[M + H]^+$ (calcd for $C_{32}H_{52}NO_{11}^+$, 626.3534).

5-Hydroxy-6-hydroxymethyl-13-hydroxyglucopiericidin A (**22**). Pale yellow oil; IR (film) ν_{max} 3392, 1670, 1200, 1134, 723 cm^{-1}; ^{1}H and ^{13}C NMR data, Tables **S2-4** and **S2-5**; HR-ESIMS *m/z* 642.3481 $[M + H]^+$ (calcd for $C_{32}H_{52}NO_{12}^+$, 642.3484).

2-Hydroxymethyl-*Δ*3, 4-glucopiericidin A (**23**). Pale yellow oil; IR (film) ν_{max} 3356, 2926, 1471, 1411, 1124, 1016, 648 cm^{-1}; ^{1}H and ^{13}C NMR data, Tables **S2-4** and **S2-5**; HR-ESIMS *m/z* 608.3444 $[M + H]^+$ (calcd for $C_{32}H_{50}NO_{10}^+$, 608.3429).

(11*S*, 12*R*) Piericidin C1 10-*O*-*β*-D-glucoside (**24**). Pale yellow oil; IR (film) ν_{max} 3354, 2932, 1587, 1468, 1412, 1126, 1074 cm^{-1}; ^{1}H and ^{13}C NMR data, Tables **S2-4** and **S2-5**; HR-ESIMS *m/z* 594.3269 $[M + H]^+$ (calcd for $C_{31}H_{48}NO_{10}^+$, 594.3273).

(11*R*, 12*S*) Piericidin C1 10-*O*-*β*-D-glucoside (**25**). Pale yellow oil; IR (film) ν_{max} 3366, 2926, 1585, 1464, 1412, 1125, 1076, 721 cm^{-1}; ^{1}H and ^{13}C NMR data, Tables **S2-4** and **S2-5**; HR-ESIMS *m/z* 594.3288 $[M + H]^+$ (calcd for $C_{31}H_{48}NO_{10}^+$, 594.3273).

13-Dimethoxy glucopiericidin A (**26**). Pale yellow oil; IR (film) ν_{max} 3358, 2926, 1670, 1200, 1136, 802, 723 cm^{-1}; ^{1}H and ^{13}C NMR data, Tables **S2-4** and **S2-5**; HR-ESIMS *m/z* 638.3535 $[M + H]^+$ (calcd for $C_{33}H_{52}NO_{11}^+$, 638.3535).

5.5 Cell Culture and Cytotoxic Bioassay. ACHN (cat. TCHu199), OS-RC-2 (cat. TCHu40) and 786-O (cat. TCHu186) cells, along with HK-2 (cat. SCSP-511) cells were purchased from Type Culture Collection of the Chinese Academy of Sciences, Shanghai, China. ACHN cells were grown and maintained in MEM medium with 10% FBS, while OS-RC-2 and 786-O cells were grown in RPMI1640 medium with 10% FBS. HK-2 cells were grown in DMEM medium with 10% FBS. Cell viability was determined by the CCK-8 (Dojindo) assay.[28] Cells were seeded at a density of 400 to 800 cells/well in 384-well plates and then treated with various concentrations of compounds or solvent control. Sorafenib was used as the positive control. After 72h of incubation, CCK-8 reagent was added, and absorbance of the triplicate tests were measured at 450 nm by an Envision 2104 multi-label reader (Perkin Elmer). Dose response curves were plotted to determine IC_{50} using Prism 5.0 (GraphPad Software Inc.).

5.6 Cell Cycle and Apoptosis Assay. Cell cycle arrest was analyzed by propidium iodide (PI) DNA staining using flow cytometry.[28] Briefly, after treatment with piericidins for 24, 48

and 72 h, respectively, cells were harvested, prepared, and then fixed overnight. The fixed cells were harvested, washed, resuspended, and finally stained with PI (Sigma-Aldrich). Cell cycle distribution was studied using an Accuri C6 (BD) flow cytometer. Cell apoptosis was analyzed using a FITC Annexin V Apoptosis Detection Kit (BD), according to the manufacturer's protocol. Cells were treated with piericidins for 24, 48 and 72 h, stained with annexin V-FITC and PI solution, examined and analyzed quantitatively using an Accuri C6 (BD) flow cytometer.

5.7 Digital Holographic Microscopy. The Holomonitor™ M4 microscope (Phase Holographic Imaging AB, Lund, Sweden) was used for imaging and tracking ACHN cell movement and morphological changes induced by PA (**1**). This technique provides long-term kinetic cellular analysis without any cell labelling. The principle behind this method is the detection of the phase shift of the probing laser light transmitting or reflecting through a cell sample and comparison to the reference light.[29] The ACHN cells were planted (2×10^5 cells) on a 6-well plate and adhered for 24h. A concentration of 50 nM PA (**1**) was added and then the field of each sample was detected under the microscope automatically. For the morphometry analysis, the color bar means the thickness of cells.

5.8 Intracellular ROS detection. The intracellular ROS were measured by flow cytometry in a BD Accuri™ C6 flow cytometer (BD Biosciences) using CellROX® Oxidative Stress Reagents (Cat no. C10422; Life technologies, USA). ACHN cells were cultured in MEM medium with 10% FBS by 24h. Then, the medium was replaced and the cells (2×10^4 cells/well) were cultured in 6-well plates, together with PA/GPA (0, 25 nM, 50 nM) in medium and incubated by 24 h. Next, the cells were collected and incubated with CellROX® Oxidative Stress Reagents 5 μM for 30 min/37 °C in darkness. BD Accuri™ C6 flow cytometer was used to analyze the cells with ROS.

5.9 Lentivirus-mediated RNA Interference. Lentivirus (Lv) expressing short hairpin RNA (shRNA) targeting PRDX1 was designed and chemically synthesized by Shanghai GeneChem Co. Ltd. (Shanghai, China), and the non-target shRNA expressing green fluorescence protein (GFP) was only used as the RNA inference (RNAi) control. Target sequences are as followed: -TGAGACTTTGAGACTAGTT- for PRDX1; -TTCTCCGAACGTGTCACGT- for vector. ACHN cell at 50-70% confluency was transfected and then selected in medium containing puromycin (1 μg/mL). After confirming the stable transfection efficiency in 72h, cells were treated with 25 nM and 50 nM PA or GPA for 24 hours.

5.10 Immunofluorescent Staining and Confocal Microscopy. ACHN cells were co-incubated with PA/GPA in 24h. After washing three times in PBS, ACHN cells were fixed in 4% paraformaldehyde for 10 min, and permeabilized with 0.5% Triton X-100 in PBS. After washing, cells were blocked with 10% FBS in 4℃ for 12h and incubated with anti-PRDX1 primary antibody overnight. Cells were washed and then incubated with fluorescein isothiocyanate-conjugated secondary antibody (green imaging) for 2 h at room temperature. DAPI staining was also performed for nucleus localization and shown in blue. Merge imaging was shown to indicate the subcellular localization of PRDX1. Cell morphology was visualized under a Zeiss fluorescence microscope (Carl Zeiss, LSM 880 with Airyscan, Germany).

5.11 SPR Assay. The surface plasmon resonance (SPR) measurement was performed on Biacore T100 system (GE Healthcare). Full-length human PRDX1 was immobilized on a CM5 chip (GE healthcare). Diluted in 10 mM Hepes (pH 7.4) for giving a concentration series, PA/GPA samples were dispensed into single-used snap-capped vials and injected across the protein and the protein-free (control) surfaces in a single step. Compound binding with PRDX1

was analyzed in a single-cycle kinetic analysis range from 1–10 μM PA and 1–20 μM GPA respectively. The K_D values were calculated using dynamic fitting equation.[30]

5.12 Molecular Docking. The Schrödinger 2017-1 suite (Schrödinger Inc., New York, NY) was employed to perform dock analysis. The PRDX1 structure was retrieved from the available crystal structure (PDB code: 2Z9S, chains a,b,c and d) and constructed following the Protein Prepare Wizard workflow in Maestro11-1. The prepared ligands were then flexibly docked into the receptor using Induce-fit module with default parameters.

5.13 Tumorigenesis Assays. Four-week old, male athymic nude (Balb/c nu/nu) mice were purchased from Guangdong Medical Lab Animal Center (China) and allowed to acclimatize for 1 week. Ten million ACHN cells in logarithmic growth phase, suspended in 0.2mL PBS on ice, were inoculated into the right flank of the nude mice. After the tumors became palpable (around 150 mm^3), mice were randomly divided into four groups, when the average weights and tumors volumes distributed equally in each group. Tumor-bearing mice were received PA (0.8 mg/kg) or GPA (0.8 mg/kg) daily by intraperitoneal injection. Sorafenib tosylate (50 mg/kg) was dissolved in Cremophor EL (Sigma) as a 10× stock solution, further diluted in PBS before use. During the exposure period the animals were kept at a temperature of 21°C at a humidity of 55% under a 12 h/12 h light/dark cycle with free access to food and water. Tumor growth was measured through calipers, and tumor volumes and body weight were in record. The calculation of tumor volumes was according to the formula $0.5 \times \text{length} \times \text{width}^2$.

5.14 Histology. When nude mice were sacrificed at day 21, tumor tissues were rapidly fixed in 4% paraformaldehyde (Sigma) at room temperature overnight. After fixation, tissues were dehydrated in ethanol with increasing concentrations up to 100%. Dehydrated specimens were

subsequently infiltrated with 100% xylene and then embedded in paraffin wax. Five μm-thick sections were cut for immune-histochemical studies, which were performed, using standard techniques.

5.15 Western Blot Analysis. ACHN cells, shPRDX1-ACHN cells and tumor tissues were lysed in RIPA buffer (Beyotime), including 50 mM Tris (pH7.4), 150 mM NaCl, 1% Triton X-100, 1% sodium deoxycholate, 0.1% SDS, sodium orthovanadate, EDTA and a protease inhibitor cocktail (Sigma). The supernatants were collected after centrifugation at 13000 rpm at 4°C for 30 min, and the quantification of protein content was estimated by BCA Protein Assay kit (Beyotime), detected with a spectrophotometer using absorption at 562 nm. Proteins (30–50 μg) were separated on 10% or 12% polyacrylamide gels and transferred to PVDF membranes using a Bio-Rad Trans-Blot wet transfer apparatus. Subsequently, the membranes were incubated with primary antibody (1:1000 for PRDX1, 1:3000 for β-Actin, 1:3000 for GAPDH) overnight after blocking with 5% nonfat milk for 2 h at room temperature. Then the appropriate HRP-conjugated secondary antibody (1:3000) was used for detection by ECL substrates.

5.16 Compliance with Ethical Standards. Animal used was permitted by the animal ethics committee of Southern Medical University. The clinical samples were collected from the Nanfang Hospital of Southern Medical University, Guangzhou, China. Informed consents were obtained from all participants. Approval for tissue collection was obtained from the ethics committee of Nanfang Hospital of Southern Medical University. Baseline clinical characteristics of human kidney samples were listed in **Table S10**.

ASSOCIATED CONTENT

Supporting Information.

This material is available free of charge via the Internet at http://pubs.acs.org. Supplementary figures and tables, structure elucidation and spectral data of compounds **1-27**, as well as their spectra (IR, MS and NMR) (PDF). Transcriptome data and bioinformatic analysis (**Tables S1~S6**) (ZIP). Molecular formula strings for **1-27** (CSV).

AUTHOR INFORMATION

Corresponding Author

* X. Zhou (E-mail: xfzhou@scsio.ac.cn)

* L. Tang (E-mail: tl405@smu.edu.cn).

Author Contributions

# X. Zhou and Z. Liang contributed equally.

X. Zhou, K. Li, W. Fang, X. Luo, S. Liao conducted chemical experiments; and Z. Liang, Y. Chen, Z. Zhan, T. Zhang, L. Tang performed the biological experiments; Y. Tian, K. Li, L. Tang performed the docking analysis; X. Zhou, S. Liu, Y. Liu, W. Fenical, L. Tang conceived and designed the project; X. Zhou, Z. Liang, and L. Tang wrote the manuscript with the assistance of all authors. All authors participated in data analyses and discussions.

Notes

The authors declare no competing financial interest.

ACKNOWLEDGMENT

This work was supported by grants from the Guangdong MEPP Funds (GDME-2018C010, 2019-017), National Natural Science Foundation of China (81673677, 21772210), Drug Innovation Major Project of China (2018ZX09735001-002-003), the Natural Science Foundation of Guangdong Province (2016A030313592), the Applied Science and Technology Research

Foundation of Guangdong Province (2016B020237005), and the Open Project of State Key Laboratory of Organ Failure Research (201802). We are grateful to Z. Xiao, A. Sun, and Y. Zhang from the analytical facilities of SCSIO.

Abbreviations

RCC, renal cell carcinoma; ccRCC, clear cell renal cell carcinoma; PA, piericidin A; GPA, glucopiericidin A; PRDX1, peroxiredoxin 1; ROS, reactive oxygen species; ECD, electronic circular dichroism; HR-ESIMS, high resolution electrospray ionization mass spectrometer; Sora, Sorafenib; bp, basepairs; DEGs, differentially expressed genes; sWGCNA, supervised weighted correlation network analysis; KEGG, Kyoto encyclopedia of genes and genomes; FDR, false discovery rate; RT-PCR, reverse transcription-polymerase chain reaction; GEO, gene expression omnibus; Kd, knockdown; shRNA, short hairpin RNA; Lv, lentivirus; shPRDX1, lentivirus PRDX1 shRNA; RNAi, RNA inference; PI, propidium iodide; K_D, dissociation equilibrium constants; SPR, surface plasmon resonance; HE, haematoxylin and eosin; TUNEL, terminal deoxynucleotidyl transferase-mediated dUTP nick end labelling; DMEM, Dulbecco's modified eagle medium; PVDF, polyvinylidene fluoride; ECL, enhanced chemiluminescence.

REFERENCES

(1) Shroff, E. H.; Eberlin, L. S.; Dang, V. M.; Gouw, A. M.; Gabay, M.; Adam, S. J.; Bellovin, D. I.; Tran, P. T.; Philbrick, W. M.; Garcia-Ocana, A.; Casey, S. C.; Li, Y.; Dang, C. V.; Zare, R. N.; Felsher, D. W., MYC oncogene overexpression drives renal cell carcinoma in a mouse model through glutamine metabolism. *Proc. Natl. Acad. Sci. U.S.A.* **2015**, *112*, 6539−6544.

(2) Varella, L.; Rini, B. I., Emerging drugs for renal cell carcinoma. *Expert. Opin. Emerg. Drugs* **2010**, *15*, 343−353.

(3) Brown, C., Targeted therapy: An elusive cancer target. *Nature* **2016**, *537*, S106-S108.

(4) Mehra, R., An insight into the "Dark Matter" of kidney cancer. *Eur. Urol.* **2018,** *74*, 764−766.

(5) Cancer Genome Atlas Research Network, Comprehensive molecular characterization of clear cell renal cell carcinoma. *Nature* **2013**, *499*, 43−49.

(6) Zhou, X.; Fenical, W., The unique chemistry and biology of the piericidins. *J Antibiot.* **2016**, *69*, 582−593.

(7) Han, X.; Liu, Z.; Zhang, Z.; Zhang, X.; Zhu, T.; Gu, Q.; Li, W.; Che, Q.; Li, D., Geranylpyrrol A and piericidin F from *Streptomyces* sp. CHQ-64 Δ*rdmF*. *J. Nat. Prod.* **2017**, *80*, 1684−1687.

(8) Shang, N. N.; Zhang, Z.; Huang, J. P.; Wang, L.; Luo, J.; Yang, J.; Peng, T.; Yan, Y.; Ma, Y. T.; Huang, S. X., Glycosylated piericidins from an endophytic streptomyces with cytotoxicity and antimicrobial activity. *J. Antibiot.* **2018**, *71*, 672−676.

(9) Schnermann, M. J.; Romero, F. A.; Hwang, I.; Nakamaru-Ogiso, E.; Yagi, T.; Boger, D. L., Total synthesis of piericidin A1 and B1 and key analogues. *J. Am. Chem. Soc.* **2006**, *128*, 11799−11807.

(10) Liu, Q.; Yao, F.; Chooi, Y. H.; Kang, Q.; Xu, W.; Li, Y.; Shao, Y.; Shi, Y.; Deng, Z.; Tang, Y.; You, D., Elucidation of piericidin A1 biosynthetic locus revealed a thioesterase-dependent mechanism of alpha-pyridone ring formation. *Chem. Biol.* **2012**, *19*, 243−253.

(11) Chen, Y.; Zhang, W.; Zhu, Y.; Zhang, Q.; Tian, X.; Zhang, S.; Zhang, C., Elucidating hydroxylation and methylation steps tailoring piericidin A1 biosynthesis. *Org. Lett.* **2014**, *16*, 736−739.

(12) Neumann, C. A.; Krause, D. S.; Carman, C. V.; Das, S.; Dubey, D. P.; Abraham, J. L.; Bronson, R. T.; Fujiwara, Y.; Orkin, S. H.; Van Etten, R. A., Essential role for the peroxiredoxin Prdx1 in erythrocyte antioxidant defence and tumour suppression. *Nature* **2003**, *424*, 561−565.

(13) Ding, C.; Fan, X.; Wu, G., Peroxiredoxin 1−an antioxidant enzyme in cancer. *J. Cell. Mol. Med.* **2017**, *21*, 193−202.

(14) Hampton, M. B.; Vick, K. A.; Skoko, J. J.; Neumann, C. A., Peroxiredoxin involvement in the initiation and progression of human cancer. *Antioxid. Redox. Signal.* **2018**, *28*, 591−608.

(15) Perroud, B.; Lee, J.; Valkova, N.; Dhirapong, A.; Lin, P. Y.; Fiehn, O.; Kultz, D.; Weiss, R. H., Pathway analysis of kidney cancer using proteomics and metabolic profiling. *Mol. Cancer* **2006**, *5*, 64.

(16) Chaiswing, L.; St Clair, W. H.; St Clair, D. K., Redox paradox: A novel approach to therapeutics-resistant cancer. *Antioxid. Redox. Signal.* **2018**, *29*, 1237−1272.

(17) Cao, J.; Schulte, J.; Knight, A.; Leslie, N. R.; Zagozdzon, A.; Bronson, R.; Manevich, Y.; Beeson, C.; Neumann, C. A., Prdx1 inhibits tumorigenesis via regulating PTEN/AKT activity. *EMBO J.* **2009**, *28*, 1505−1517.

(18) Wang, X.; He, S.; Sun, J. M.; Delcuve, G. P.; Davie, J. R., Selective association of peroxiredoxin 1 with genomic DNA and COX-2 upstream promoter elements in estrogen receptor negative breast cancer cells. *Mol. Biol. Cell* **2010**, *21*, 2987-2995.

(19) Luo, W.; Chen, I.; Chen, Y.; Alkam, D.; Wang, Y.; Semenza, G. L., PRDX2 and PRDX4 are negative regulators of hypoxia-inducible factors under conditions of prolonged hypoxia. *Oncotarget* **2016**, *7*, 6379−6397.

(20) Min, Y.; Kim, M. J.; Lee, S.; Chun, E.; Lee, K. Y., Inhibition of TRAF6 ubiquitin-ligase activity by PRDX1 leads to inhibition of NF-κB activation and autophagy activation. *Autophagy* **2018**, *14*, 1347−1358.

(21) Matsumura, T.; Okamoto, K.; Iwahara, S.; Hori, H.; Takahashi, Y.; Nishino, T.; Abe, Y., Dimer-oligomer interconversion of wild-type and mutant rat 2-Cys peroxiredoxin: disulfide formation at dimer-dimer interfaces is not essential for decamerization. *J. Biol. Chem.* **2008**, *283*, 284−293.

(22) Lee, W.; Choi, K. S. Riddell, J.; Ip, C.; Ghosh, D.; Park, J. H.; Park, Y. M., Human peroxiredoxin 1 and 2 are not duplicative proteins: the unique presence of Cys83 in Prx1 underscores the structural and functional differences between Prx1 and Prx2. *J. Biol. Chem.* **2007**, *282*, 22011−22022.

(23) Yan, Q.; Li, R.; Xin, A.; Han, Y.; Zhang, Y.; Liu, J.; Li, W.; Di, D., Design, synthesis, and anticancer properties of isocorydine derivatives. *Bioorg. Med. Chem.* **2017**, *25*, 6542−6553.

(24) Engl, T.; Kroiss, J.; Kai, M.; Nechitaylo, T. Y.; Svatos, A.; Kaltenpoth, M., Evolutionary stability of antibiotic protection in a defensive symbiosis. *Proc. Natl. Acad. Sci. U.S.A.* **2018**, *115*, E2020−E2029.

(25) Reczek, C. R.; Chandel, N. S., ROS promotes cancer cell survival through calcium signaling. *Cancer Cell* **2018**, *33*, 949−951.

(26) Forshaw, T. E.; Holmila, R.; Nelson, K. J.; Lewis, J. E.; Kemp, M. L.; Tsang, A. W.; Poole, L. B.; Lowther, W. T.; Furdui, C. M., Peroxiredoxins in cancer and response to radiation therapies. *Antioxidants* **2019**, *8*, 11.

(27) Evens, A. M.; Prachand, S.; Shi, B.; Paniaqua, M.; Gordon, L. I.; Gartenhaus, R. B., Imexon-induced apoptosis in multiple myeloma tumor cells is caspase-8 dependent. *Clin. Cancer Res.* **2004**, *10*, 1481−1491.

(28) Tan, Y.; Yang, B.; Lin, X.; Luo, X.; Pang, X.; Tang, L.; Liu, Y.; Li, X.; Zhou, X., Nitrobenzoyl sesquiterpenoids with cytotoxic activities from a marine-derived *Aspergillus ochraceus* fungus. *J. Nat. Prod.* **2018**, *81*, 92−97.

(29) Peter, B.; Nador, J.; Juhasz, K.; Dobos, A.; Korosi, L.; Szekacs, I.; Patko, D.; Horvath, R., Incubator proof miniaturized Holomonitor to *in situ* monitor cancer cells exposed to green tea polyphenol and preosteoblast cells adhering on nanostructured titanate surfaces: validity of the measured parameters and their corrections. *J. Biomed. Opt.* **2015**, *20*, 067002.

(30) Wang, J.; Chen, F.; Liu, Y.; Liu, Y.; Li, K.; Yang, X.; Liu, S.; Zhou, X.; Yang, J., Spirostaphylotrichin X from a marine-derived fungus as an anti-influenza agent targeting RNA polymerase PB2. *J. Nat. Prod.* **2018**, *81*, 2722−2730.

Table of Contents graphic: